Available online at www.sciencedirect.com
ScienceDirect
Journal of Molecular Graphics and Modelling 25 (2006) 103–115
Journal of Molecular Graphics and Modelling
www.elsevier.com/locate/JMGM

β-Hairpins with native-like and non-native hydrogen bonding patterns could form during the refolding of staphylococcal nuclease

Sunita Patel [a], Prakash Sista [a], Petety V. Balaji [b], Yellamraju U. Sasidhar [a,b,*]

[a] *Department of Chemistry, Indian Institute of Technology Bombay, Powai, Mumbai 400076, India*
[b] *School of Biosciences & Bioengineering, Indian Institute of Technology Bombay, Powai, Mumbai 400076, India*

Received 9 July 2005; received in revised form 19 November 2005; accepted 20 November 2005
Available online 28 December 2005

Abstract

Refolding of staphylococcal nuclease has been studied recently by hydrogen–deuterium exchange and NMR spectroscopy. These studies infer that β-hairpin formed by strand 2 and strand 3 connected by reverse turn forms early during the refolding of nuclease. Typically, hydrogen–deuterium exchange NMR techniques are usually carried out on a time scale of milliseconds whereas β-hairpins are known to fold on a much shorter time scale. It follows that in the experiments, the hydrogen–deuterium exchange protection patterns could be arising from a significant population of fully formed hairpins. In order to demonstrate it is the fully formed hairpins which gives rise to the hydrogen–deuterium exchange protection patterns, we have considered molecular dynamics simulation of the peptide ^{21}DTVKLM*YKGQ*PMTFR^{35} from staphylococcal nuclease corresponding to the β-hairpin region, using GROMOS96 force field under NVT conditions. Starting from unfolded conformational states, the peptide folds into hairpin conformations with native-like and non-native hydrogen bonding patterns. Subsequent to folding, equilibrium conditions prevail. The computed protection factors and atom depth values, at equilibrium, of the various amide protons agree qualitatively with experimental observations. A collection of molecules following the trajectories observed in the simulations can account for experimental observations. These simulations provide a molecular picture of the formed hairpins and their conformational features during the refolding experiments on nuclease, monitored by hydrogen–deuterium exchange.

Keywords: Atom depth; Hydrogen–deuterium exchange; Peptide; GROMACS; GROMOS96; Protein folding; Hydrogen bonds

1. Introduction

β-Hairpin is an important secondary structural element in the protein structure. β-Hairpin peptides from many protein systems have been studied with both experimental and molecular dynamics (MD) simulation techniques [1–14]. These studies comment on the mechanism of hairpin formation and its stability. However, in many cases it is not clear whether the formation of the β-hairpin does actually take part on the folding pathway or not. In order to characterize the formation of a hairpin on a folding pathway, we have, therefore, considered a β-hairpin peptide model from staphylococcal nuclease from a region, which is known to have folded early during the refolding.

The sequence ^{21}DTVKLM*YKGQ*PMTFR^{35} adopts a β-hairpin structure in the crystal structure of staphylococcal nuclease (PDB code 1SNC) [15]. The sequence YKGQ adopts a type I′ turn conformation and connects strands 2 and 3 forming a β-hairpin. Refolding of staphylococcal nuclease is monitored by hydrogen–deuterium (H–D) exchange techniques using ^{1}H NMR by two experimental groups [16,17]. H–D exchange technique can only detect whether a particular region of the protein is folded or not; it cannot detect the existence of secondary structures directly. Out of 15 residues, which are protected from exchange, eight residues are located in the hairpin region [16]. Both the studies infer from the pattern of H–D exchange protection that formation of the hairpin might be an early event in the refolding of staphylococcal nuclease. Note that refolding studies using H–D exchange NMR technique are usually carried out on a time scale of milliseconds. It is known experimentally that β-hairpins form on a much shorter time scales. The time scale ranges from

* Corresponding author. Tel.: +91 22 2576 7179; fax: +91 22 2576 7152.
E-mail address: sasidhar@iitb.ac.in (Y.U. Sasidhar).

1093-3263/$ – see front matter © 2005 Elsevier Inc. All rights reserved.
doi:10.1016/j.jmgm.2005.11.007

nanoseconds to microseconds depending upon the peptide system and refolding conditions [6,18,19]. This implies that in the H–D exchange studies referred to, considerable hairpin population might have already formed during the dead time of the H–D exchange experiment. Therefore, the H–D exchange protection pattern of strand 2 and 3 of the nuclease might be coming from a sizable population of formed hairpins.

In this study, to demonstrate that it is the fully formed hairpins, which give rise to the observed H–D exchange protection factors, we have considered MD simulations of the hairpin peptide Ac-^{2}DTVKLMYKGQPMTFR^{16}-NMe from staphylococcal nuclease. In order to generate the hairpin conformation without any bias, we have considered two starting conformations: fully extended conformation and polyproline II conformation. We considered polyproline II conformation as a model for the unfolded state since some of the recent spectroscopic studies of unfolded polyalanine peptides suggest that they sample polyproline II helical conformation [20–23]. Recent simulations also find that unfolded state of polyalanine is a segmented polyproline II helical conformation, which is also a preferred conformation [24,25]. We further considered a mutant version of the peptide (D2N) to assess the effect of the mutation on the stability of the folded hairpin. This and other mutations else where in the native nuclease are known to increase its thermo-stability [26]. Starting from unfolded conformations, hairpins form with native-like and non-native hydrogen bonding patterns and subsequently equilibrium conditions prevail. The conformational properties of these fully formed hairpins during equilibrium are compared to experimental H–D exchange protection patterns and protection factors. We find that a good correlation exist between computed protection factors, observed hydrogen bonding patterns and experimental results. These results suggest that the experimental protection factors observed in the NMR experiments could have arisen from the formed hairpin molecules with native-like and non-native hydrogen bonding patterns. Thus, these simulations provide a molecular picture of the formed hairpins and their conformational features during the refolding experiments on nuclease, monitored by H–D exchange.

2. Methods

MD simulations are performed on the peptide Ac-^{2}DTVKL-MYKGQPMTFR^{16}-NMe in explicit solvent. The ends of the peptides are protected by the CH_3CO-group (Ac) at the N-terminus and the $-NHCH_3$ group (NMe) at the C-terminus. In all the simulations reported the peptide is given an initial conformation which is either fully extended or a polyproline II conformation. In fully extended conformation all ϕ, ψ and side chain dihedral angles are set to 180° except for χ_1 which is set at 60°. In the case of proline only ψ is set at 180°. Similarly, D2N mutant of the peptide is generated in fully extended conformation using Deep View [27]. The peptide in polyproline II conformation is also generated using Deep View by setting all backbone dihedral angles of the β-hairpin region from crystalline nuclease (PDB code 1SNC) to polyproline II values ($\phi = -76°$ and $\psi = 149°$). We considered D2 in protonated or uncharged form since the refolding of staphylococcal nuclease is carried out under acidic conditions [16,17]. Each of the residues K5, K9 and R16 is carrying a unit charge. Thus, the peptide has a total charge of +3 units.

The following abbreviations are used to indicate the simulations performed:

Extended, Simulation with initial extended conformation of the peptide in a cubic box.
PPII, Simulation with initial polyproline II conformation in a cubic box.
D2N, Simulation with initial extended conformation with D2 mutated to N2 in a cubic box.
ER, Simulation with initial extended conformation in a rectangular box.

One simulation run is performed for each initial conformation. In Extended, D2N and PPII simulations the simulation box is cubic with sides of 7.41, 7.41 and 7.18 nm, respectively, and contained 13,494, 13,494 and 12,272 SPC water molecules [28], respectively, solvating the peptide. For ER simulation, the box has the dimensions 7.34 nm × 3.70 nm × 3.40 nm and contained 2996 SPC water molecules along with the peptide. All the simulations are performed with periodic boundary conditions.

The electrostatic interactions are treated by PME method [29,30] with a Coulomb cut-off of 1 nm, Fourier spacing of 0.12 nm and an interpolation order of 4. No neutralizing counterions are added since PME methodology adds a uniform background neutralizing charge [31,32]. The van der Waals interactions are treated using Lennard-Jones potential and a switching function with a cut-off distance of 1 nm and a switching distance of 0.9 nm.

The potential energy of the peptide in water is minimized using steepest descent algorithm with a tolerance of 100 kJ mol^{-1} nm^{-1} and convergence is obtained in all the cases. Subsequent to energy minimization, position restrained molecular dynamics is carried out for 50 ps using a reference temperature of 300 K. In this procedure, the atomic positions of the peptide are restrained and the water molecules are allowed to equilibrate around the peptide, to remove the solvent holes. Initial velocities required to start the procedure are generated conforming to Maxwell velocity distribution at 300 K. Following these equilibration procedures, MD is initiated. A time step of 2 fs is used for integrating the equations of motion. LINCS algorithm is used to constrain the bonds [33]. Coordinates are saved every 250 steps or 0.5 ps and velocities are saved every 500 steps or 1 ps. The peptide and the solvent are separately coupled to a Berendsen temperature bath [34] using a time constant of 0.1 ps. All the simulations are done under NVT conditions for a period 30 ns or more.

MD simulations are performed using the software GROMACS (version 3.1.4) [35] and GROMOS96 (ffG43a1) force field [36,37] on dual xeon processor based machines running Red-Hat Linux 8 (http://www.redhat.com). Except for polar hydrogens like –NH, –OH and aromatic ring hydrogens, united atom approximation is used. The analysis tools provided by

GROMACS software are used to analyze the data. Clustering analysis of the conformations sampled during simulations is performed using an algorithm due to Daura et al. [38] as implemented in GROMACS with a cut-off of 0.15 nm. Matlab (http://www.mathworks.com) and Octave (http://www.octave.org) are also used for some of the analyses. Most of the graphs and figures are generated using Xmgrace (http://plasma-gate.weizmann.ac.il/Grace), Matlab and VMD [39].

The following conformational properties of the peptide are monitored.

1. Radius of gyration (R_g) of the backbone atoms.
2. Hydrophobic radius of gyration (R_{gh}) of hydrophobic side chains (excluding C_α atoms).
3. End-to-end distance (the distance between D2 (C_α) and R16 (C_α) atoms).
4. Root mean square deviation (RMSD) with respect to backbone conformation of the hairpin in crystalline nuclease (PDB code 1SNC) excluding N-terminal Ac-D2 and C-terminal R16-NMe residues following Daura et al. [38,40].
5. Hydrogen bonds involving mainchain NH and CO groups (a hydrogen bond is considered to be present between NH and CO if the distance between the H and O atoms is less than 0.26 nm).
6. Hydrogen bonds involving mainchain NH and CO groups and solvent water.
7. Potential energy of the peptide.
8. Potential energy of the peptide and solvent interactions.
9. Atom depth: this is defined as the distance between a protein atom and the nearest water molecule [41,42]. It has been found that the depths of amide N-atoms in lysozyme are correlated with the experimentally determined amide H–D exchange rates [43]. We therefore used the depth of the amide proton as a measure of its protection from H–D exchange.

3. Results

3.1. The peptide Ac-^{2}DTVKLMYKGQPMTFR^{16}-NMe folds into a hairpin conformation and subsequently equilibrium conditions prevail for the duration of simulation

The conformational parameters such as R_g, R_{gh}, end-to-end and RMSD distance are monitored as a function of time for all the simulations and the results are shown in Fig. 1. All conformational parameters start with relatively higher values and fall to low values within 5 ns. Thereafter they maintain steady values, suggestive of equilibrium. The R_g value decreases from a high value of 1.4 nm to a low value of ~0.7 nm within 5 ns in all the simulations and thereafter it hovers around 0.7 nm (Fig. 1a), indicating that peptide has adopted a compact conformation within a short time and the compact conformation is retained during the equilibrium period. This is also evident from Table 1, which summarizes the average values of the various conformational parameters observed in the simulations during the equilibrium. The hydrophobic radius of gyration (R_{gh}) falls to a low value of ~0.55 nm within 5 ns (Fig. 1b), suggesting that the

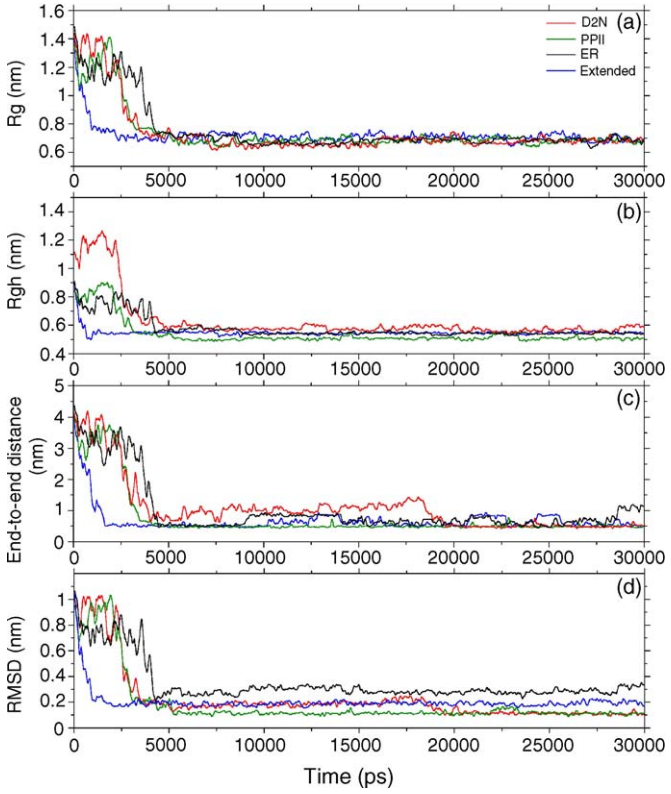

Fig. 1. The conformational parameters R_g (a); R_{gh} (b); end-to-end distance (c); and RMSD (d) as a function of time in all the simulations. Red line indicates D2N simulation; green line indicates PPII simulation; black line indicates ER simulation; blue line indicates Extended simulation. A running average over 200 data points is plotted for all the graphs, for visual clarity.

compact conformation attained by the peptide is possibly driven by hydrophobic association. Thereafter, the values of R_{gh} are more or less steady for the duration of the simulations. This is also evident from R_{gh} values in Table 1, indicating that the existence of similar hydrophobic association in the compact conformation of the folded peptide. The end-to-end distance decreases significantly from ~4.5 to 0.6 nm within 5 ns (Fig. 1c), suggesting that N- and C-terminal ends of the peptide have come closer due to the folding of the peptide. However, during the equilibrium, the end-to-end distances values vary from simulation to simulation (Fig. 1c and Table 1), possibly because of the fluctuating free ends, which leads to the differences in their average values. In D2N simulation relatively larger fluctuations are observed up to 18 ns thereafter the end-to-end distance values settle around ~0.5 nm. This can be attributed to fraying at the end of the folded peptide. We further note that RMSD values also falls below ~0.2 nm within 5 ns (Fig. 1d), indicating that the peptide is adopting a conformation similar to that of hairpin conformation in crystalline nuclease. The RMSD value decreases to a low value of ~0.12 nm in PPII simulation, whereas in Extended, D2N and ER simulations RMSD values are 0.19, 0.15 and 0.29 nm, respectively (Fig. 1d and Table 1), indicating that hairpin conformations sampled in these simulations are similar to that in crystalline nuclease, since the hairpin conformation of the crystalline nuclease is used as the reference conformation for the computation of root mean square deviation. In all the simulations, formation of inter-strand backbone

Table 1
Average values of the various conformational parameters and their standard deviations, observed during the equilibrium period (10–30 ns) of the simulations

Simulation	R_g (nm)	R_{gh} (nm)	End-to-end distance (nm)	RMSD (nm)	Number of inter-strand backbone hydrogen bonds	Number of peptide-solvent hydrogen bonds
Extended	0.70 ± 0.03	0.55 ± 0.01	0.64 ± 0.14	0.19 ± 0.02	6 ± 1	18 ± 3
PPII	0.68 ± 0.02	0.51 ± 0.01	0.50 ± 0.06	0.12 ± 0.02	7 ± 1	18 ± 2
D2N	0.67 ± 0.03	0.57 ± 0.02	0.77 ± 0.31	0.15 ± 0.05	5 ± 1	18 ± 3
ER	0.68 ± 0.02	0.54 ± 0.01	0.71 ± 0.17	0.29 ± 0.03	5 ± 1	18 ± 3

hydrogen bonds is associated with the loss of peptide solvent hydrogen bonds (Fig. 2). This indicates that as the peptide is folding the NH and CO groups of the backbone, which are solvated when peptide is unfolded, become in accessible to the solvent due to the formation of inter-strand backbone hydrogen bonds. The number of inter-strand backbone hydrogen bonds and the number of hydrogen bonds between the peptide and the solvent did not vary much from simulation to simulation (Table 1). Since in a given simulation, all the conformational parameters monitored decreases simultaneously, the peptide undergoes a cooperative conformational change to form a hairpin conformation and during the equilibrium, conformational parameters sampled similar values in all the simulations.

3.2. Hairpins with native-like and non-native hydrogen bonding patterns formed in the simulations

The peptide, starting from various unfolded conformations folds into hairpins with native-like and non-native hydrogen bonds. Following folding, hairpin conformation is maintained and equilibrium conditions prevail. The hydrogen bonding pattern observed during the equilibrium period of the simulations are summarized in Fig. 3. The backbone hydrogen bonds observed in the hairpin structure of the crystalline nuclease are Q11:H-Y8:O, Y8:H-Q11:O, M13:H-L6:O, L6:H-M13:O, F15:H-V4:O and V4:H-F15:O (Fig. 3a). Similar native-like hydrogen bonding patterns are observed in the PPII and D2N simulations (Fig. 3b). However, in Extended simulation non-native hydrogen bonding pattern is observed. The observed hydrogen bonds are Q11:H-K9:O, K9:H-Q11:O, M13:H-M7:O, M7:H-M13:O, F15:H-K5:O and K5:H-F15:O (Fig. 3b). Whereas, in ER simulation both native-like (L6:H-M13:O) and non-native (Q11:H-K9:O, M13:H-M7:O, M7:H-M13:O, L6:H-T14:O, R16:H-V4:O) hydrogen bonding patterns are observed (Fig. 3b). Fig. 3b also highlights the positions of the hydrophobic residues in the folded hairpins. This indicates, schematically, hydrophobic clusters in the folded hairpin structures in various simulations.

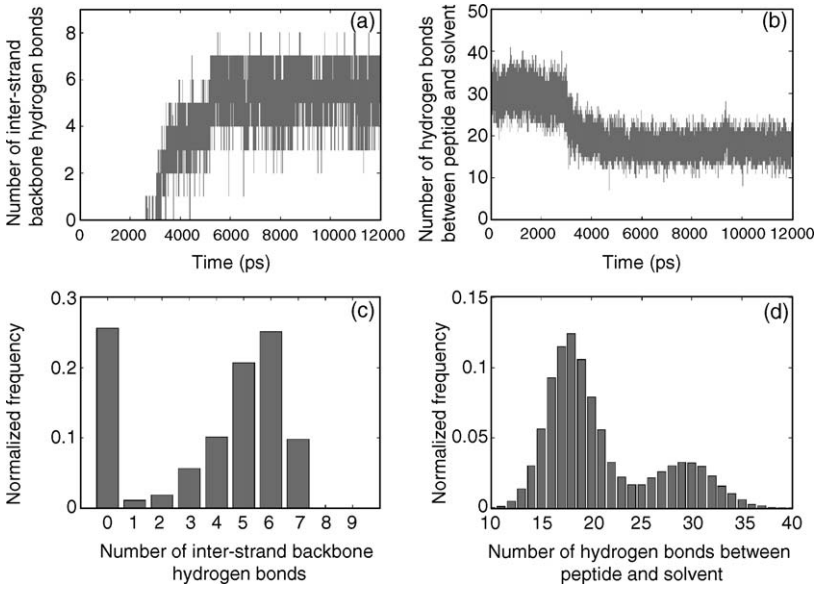

Fig. 2. Number of hydrogen bonds as a function of time and their distribution in the PPII simulation. (a) Number of inter-strand backbone hydrogen bonds of the peptide vs. time during 0–12 ns. The number of hydrogen bonds increases as the peptide folds. (b) At the same time, the number of hydrogen bonds between backbone NH, CO groups and the solvent water decreases. (c) A histogram representation of panel-a showing the distribution of backbone hydrogen bonds during 12 ns of simulation. There are two peaks in the distribution. The peak at 0 is from time frames where the peptide is unfolded. The second distribution with a maxima at 6 hydrogen bonds is from the time frames where the peptide is folding and has folded. We infer that during folding and shortly thereafter, the peptide samples six hydrogen bonds on the average. (d) A histogram representation of panel-b showing the distribution of hydrogen bonds between the peptide backbone and solvent. There are two distributions with peaks at 18 and 30 hydrogen bonds. The first distribution is from the time frames where the peptide is folding and the second distribution is from the time frames where the peptide is unfolded and thus has many hydrogen bonds with the solvent.

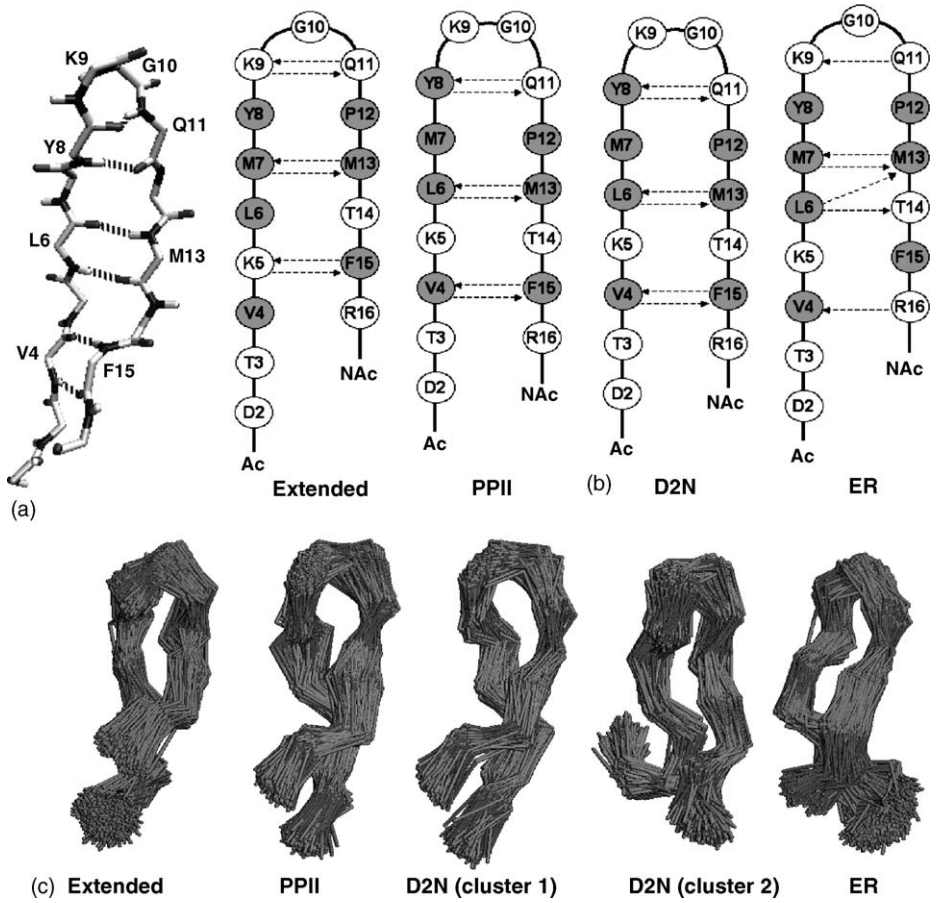

Fig. 3. Pattern of inter-strand backbone hydrogen bonding observed for the hairpin in: (a) the crystal structure of staphylococcal nuclease (PDB code 1SNC) (with the numbering of the residues as defined in Section 2); (b) Extended, PPII, D2N and ER simulations. The pattern of hydrophobic residues present in the folded peptide is also shown schematically in gray color. The most populated conformational clusters observed in the simulations are shown in panel c (only backbone is shown). The other conformational clusters (not shown), which are populated to a lesser extent are also hairpin like. Native-like hydrogen bonding pattern is observed in PPII and D2N simulations whereas non-native hydrogen bonding pattern is observed in Extended simulation. In ER simulation both native-like and non-native hydrogen bonds are observed. Arrows represent hydrogen bonds with tails at donors (NH) and heads at acceptors (CO).

The most populated conformational clusters from Extended, PPII and ER simulations are sampled 60, 76 and 57% of the time, respectively, and are shown in Fig. 3c. These are essentially hairpin conformations. In D2N simulation, two major clusters, cluster 1 and cluster 2 sample 32 and 15% of the time, respectively, and are shown in Fig. 3c. The conformations in cluster 2 of the D2N simulation have hairpin like structure but with frayed ends (Fig. 3c) and have hydrogen bonding patterns and reverse turn, similar to those in cluster 1 except for the last tail hydrogen bond (V4:H-F15:O) which is observed only in cluster 1. The backbone conformations in cluster 1 of D2N simulation and the cluster of PPII simulations are observed to be similar (Fig. 3c). In PPII and D2N simulations, hairpin conformations with type I′ reverse turn formed by ^{8}YKGQ^{11} residues are observed, whereas in Extended and ER simulations, the observed hairpin samples γ-turn formed by ^{9}KGQ^{11} residues.

3.3. Mechanism of hairpin formation in Extended simulation

The R_g and RMSD values decrease continuously with time during the initial 2 ns period. The conformations sampled during this time are shown in the contour representation in the R_g-RMSD space (Fig. 4a). There are five different regions of R_g-RMSD space, which are relatively highly populated. These regions are labeled I_1 to I_5. Each region represents a cluster of conformations. Since R_g and RMSD decrease with time monotonically, these regions are also separated temporally. Since these regions are populated transiently during the course of the folding, they may be thought of as representing conformational forms, sampling low barrier free energy minima on their way to final equilibrium state, which represents the folded hairpin conformation (inset in Fig. 4a). The sequence of these conformational forms in time can therefore represent the folding mechanism.

The first inter-strand backbone hydrogen bond is formed between M7 NH and M13 CO at about 960 ps. This event is preceded by a conformational collapse of the peptide: the R_g of the peptide falls from an initial value of 1.52 to 0.8 nm before 960 ps (Fig. 4b). R_{gh} also falls from an initial value of 1 nm to a low value of 0.55 nm (Fig. 4b), suggesting that peptide has undergone conformational collapse driven by hydrophobic interactions. The hydrophobic association seems to be initiated by the hydrophobic contact between M7 and P12 at about

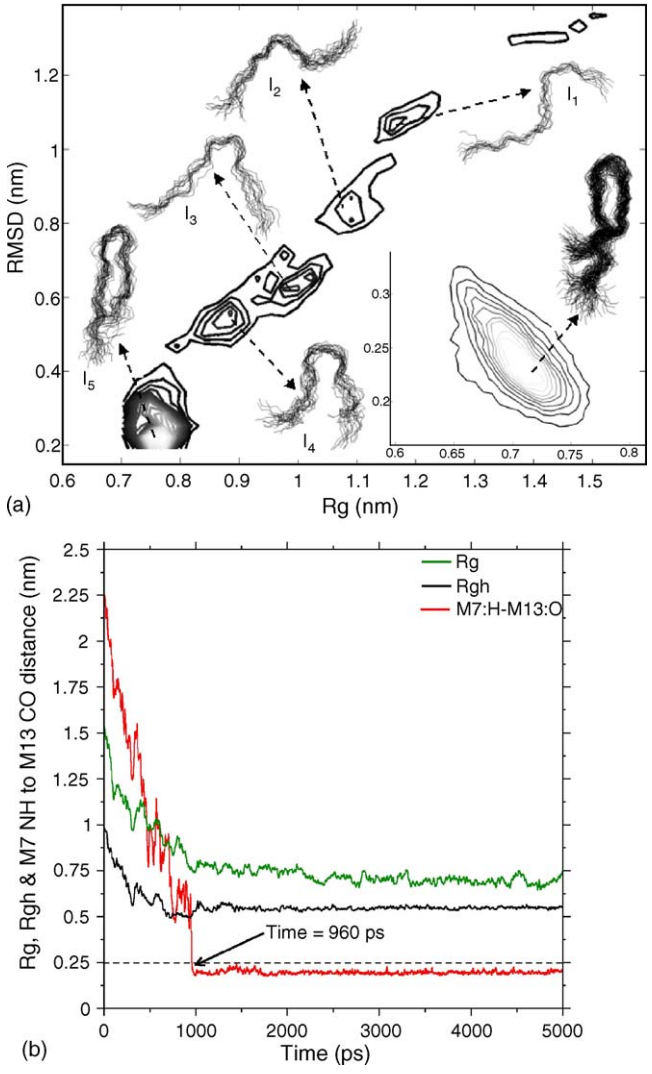

Fig. 4. The relative sampling of the R_g and RMSD values during the initial 2 ns period shown in a contour representation along with the observed transient conformational clusters (a); and the formation of first hydrogen bond takes place after the development of a compact hydrophobic cluster in Extended simulation (b). (a) The conformational clusters I_1–I_5 are sampled sequentially in time. Inset shows the conformational cluster sampled during equilibrium (10–30 ns period); this conformation differs from that sampled by cluster I_5 in that it has one additional backbone hydrogen bond on the average and is more compact and has a right-handed twist. (b) R_g, R_{gh} and M7 NH to M13 CO distance as a function of time. The M7:H-M13:O hydrogen bond forms at about 960 ps. R_g and R_{gh} attain low values of ∼0.80 and 0.55 nm, respectively, before the formation of the first hydrogen bond (M7:H-M13:O) (running averages over 20 data points are shown for visual clarity).

500 ps. This conformational form corresponds to I_3 state of Fig. 4a. Subsequently, other hydrophobic residues M13, F15, L6 and V4 also associate with the initial hydrophobic contact pair, forming a compact conformational state represented by I_4 in Fig. 4a. This event brings the opposite β-strands together leading to the formation of I_5 conformational state (Fig. 4a). At this point hydrogen bonds begin to form. The first hydrogen bond (M7:H-M13:O) forms in the middle of the hairpin, following the formation of compact hydrophobic association. The remaining hydrogen bonds which lie on both the sides of the middle hydrogen bond form subsequently in a middle-of-the-hairpin to out-wards manner. The hydrogen bonding pattern observed in the simulation is non-native. Thus, hydrophobic interactions play an important role in initiating the folding of the hairpin.

3.4. Mechanism of hairpin formation in PPII simulation

The peptide starting from the polyproline II initial conformation (Fig. 5a), remains in unfolded state for a period of about 2 ns. The residues Y8 and P12 form a hydrophobic contact at about 2.2 ns (Fig. 5b) with a C_α–C_α distance of 0.6 nm. Following this initial hydrophobic contact, association of other hydrophobic residues such as L6, M13 and F15 takes place, giving rise to a hydrophobic cluster (Fig. 5c and d). The hydrogen bonds in the turn region (Q11:H-Y8:O, Y8:H-Q11:O) are the first ones to form. This is followed by the appearance of a middle hydrogen bond (M13:H-L6:O). Eventually other hydrogen bonds also form in a top-to-bottom manner (Fig. 6) completing the hairpin formation (Fig. 5e and f). The hydrogen bonds form cooperatively, closing the hairpin by zipping from top to bottom (Fig. 6). The resulting hairpin has a right-handed twist with native-like hydrogen bonding pattern similar to that of hairpin conformation in crystalline nuclease (Fig. 3).

3.5. Mechanism of hairpin formation in D2N simulation

In this simulation, the mutant peptide (D2N) folds in a way similar to that observed in PPII and Extended simulations. The folding of the peptide is initiated by a hydrophobic contact between Y8 and P12 as in PPII simulation (Fig. 5b) at about 2.4 ns. Following this, the side chains of L6, M13 and F15 associate, leading to a compact hydrophobic cluster. A non-native hydrogen bond (Y8:H-L6:O) appears in the middle of the cluster at about 3.5 ns. Within a very short interval of time, the non-native hydrogen bond is replaced by a native-like hydrogen bond M13:H-L6:O. This is followed by the appearance of other native-like inter-strand backbone hydrogen bonds on both sides of the middle hydrogen bond as in Extended simulation. The hairpin observed in the simulation has native-like hydrogen bonding pattern. The D2N mutation does not seem to have affected the folding of the hairpin. As the mechanism shows, the mutated residue does not take part in guiding the folding of the hairpin.

3.6. Mechanism of hairpin formation in ER simulation

In the ER simulation, an initial hydrophobic contact forms between Y8 and P12 at about 445 ps. However, the hydrophobic association does not develop and the initial contact breaks up. Subsequently, a non-productive hydrophobic association takes place at about 3.81 ns (Fig. 7a), which then breaks at about 3.99 ns without the development of any hydrogen bonds (Fig. 7b). However, a second event of hydrophobic association, which occurs at about 4.15 ns (Fig. 7c), proves to be productive and leads to a more compact hydrophobic cluster (Fig. 7d). Following this event, hydrogen bonds begin to form between the opposite strands and

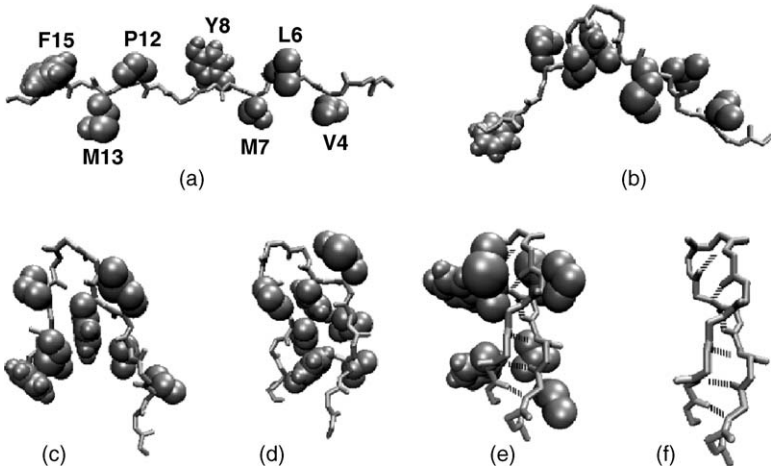

Fig. 5. Mechanism of hairpin formation in PPII simulation. The atoms of hydrophobic side chains V4, L6, M7, Y8, P12, M13 and F15 are represented as spheres with van der Waals radii. (a) Initial conformation showing hydrophobic side chains. The backbone is set to polyproline II conformation. (b) An initial hydrophobic contact between Y8 and P12 takes place at about 2.21 ns. (c) Hydrophobic association between L6, Y8, M13 and F15 at about 2.82 ns. (d) Compact hydrophobic cluster at about 2.96 ns. (e) Folded hairpin conformation with six hydrogen bonds at about 5.22 ns. (f) Same as (e) depicting only backbone.

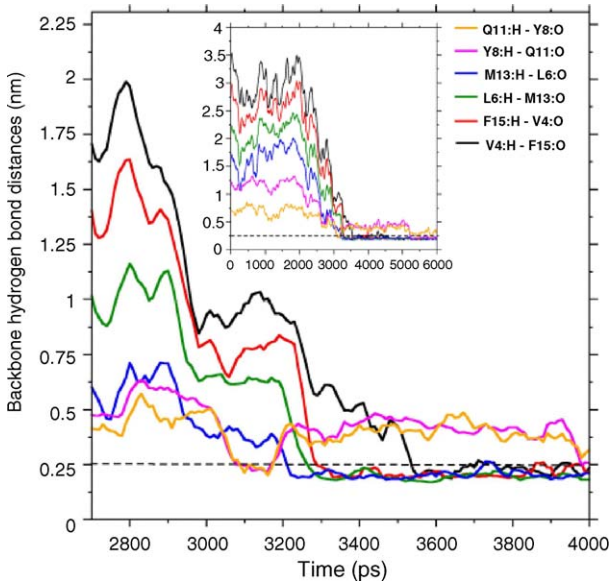

Fig. 6. Formation of inter-strand backbone hydrogen bonds in a top-to-bottom manner in PPII simulation. Running average over 50 data points is shown for the sake of clarity. Inset shows cooperative formation of the hydrogen bonds. The hydrogen bonds Q11:H-Y8:O and Y8:H-Q11:O form simultaneously at around 3.07 ns; M13:H-L6:O forms at about 3.21 ns; L6:H-M13:O forms at about 3.26 ns; F15:H-V4:O forms at about 3.29 ns; V4:H-F15:O forms at about 3.53 ns. A dotted line at 0.26 nm is shown to indicate hydrogen bonding distance.

eventually the hairpin forms with both native-like and non-native hydrogen bonding patterns (Fig. 3b).

3.7. Lennard-Jones interactions contribute significantly to the stability of the folded hairpins

The potential energy of the peptide decreases, following folding of the peptide. Table 2 shows the drop in potential energy and its Lennard-Jones and Coulomb components. The drop is calculated for PPII, D2N and ER simulations where the energy sampled a steady average value during pre-folded and post-folded times. The drop in potential energy has more contribution from Lennard-Jones interactions than from Coulomb interactions (Table 2). Thus, the Lennard-Jones interactions seem to contribute significantly to the stability of the folded hairpin observed during the equilibrium whereas Coulomb interactions, via hydrogen bonds, may have a role of aligning the strands appropriately for better packing interactions. As discussed later hydrophobic association whose energetic contribution comes largely from Lennard-Jones interactions needs to be supported by electrostatic interactions in the form of hydrogen bonds. It may be noted that the drop in energy is relatively less for the case of D2N simulation.

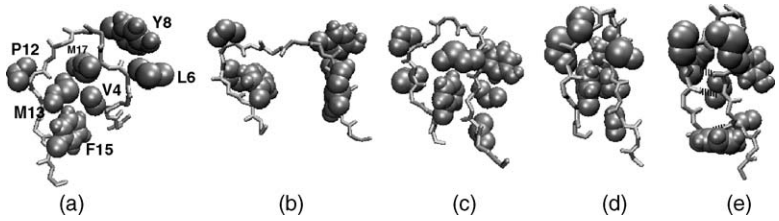

Fig. 7. Mechanism of hairpin formation in ER simulation. The atoms of hydrophobic side chains V4, L6, M7, Y8, P12, M13 and F15 are represented as spheres with van der Waals radii. (a) Non-productive hydrophobic association at about 3.81 ns. (b) Hydrophobic association breaks up around 3.99 ns (c). Hydrophobic association developed again around 4.15 ns and this turns out to be productive. This association leads to a compact hydrophobic cluster at about 4.18 ns (d). Folded hairpin conformation at about 4.33 ns with three hydrogen bonds (e).

Table 2
The potential energy of the peptide along with its LJ and Coulomb components in PPII, D2N and ER simulations

Simulation	Potential energy of the peptide (kJ/mol)			LJ energy (kJ/mol)			Coulomb energy (kJ/mol)		
	Pre-folded	Post-folded	Drop	Pre-folded	Post-folded	Drop	Pre-folded	Post-folded	Drop
PPII	1432 ± 37	1169 ± 38	263	−215.2 ± 18.9	−390.6 ± 21.7	175.4	1159 ± 25	1072 ± 25	87
D2N	1326 ± 37	1118 ± 42	208	−216.8 ± 19.7	−379.8 ± 24.4	163	1050 ± 23	1006 ± 26	44
ER	1417 ± 35	1172 ± 39	246	−223.5 ± 20.7	−387.4 ± 21.3	163.9	1151 ± 23	1067 ± 29	84

Average values with standard deviations are shown for pre-folded and post-folded times along with drop in energies following folding.

3.8. Formation of backbone hydrogen bonds is accompanied by a rise in the atom depth values of the corresponding donor amide protons

As the peptide is folding, the atom depth (see Section 2 for the definition of atom depth) of an amide proton shows a rise in its value (∼0.2–0.4 nm) around the time the amide proton takes part in hydrogen bonding with an acceptor group CO (Fig. 8), suggesting that the amide proton has moved away from the solvent and thus became solvent shielded. Such a solvent shielded proton could be protected from H–D exchange. Those amide protons which are not taking part in hydrogen bonding interactions maintained a steady atom depth values around ∼0.2 nm (Fig. 8). Thus, there seems to be a good correlation between backbone hydrogen bond formation and the rise in atom depth values of corresponding donor amide protons. By and large, all the backbone amides involved in hydrogen bonding displayed higher atom depth values following folding during the equilibrium in all the simulations (Table 3).

3.9. The H–D exchange protection factors are computed from simulations during the equilibrium

In our simulations, the hydrogen exchange protection factors are computed using Eq. (4) of Alexandrescu et al. [44].

$$K_{op} = \frac{[OPEN]}{[CLOSED]}$$

Here, K_{op} represents the equilibrium constant for the process where a hydrogen bond opens and closes under equilibrium conditions. [OPEN] and [CLOSED] refer to the concentration of ''open'' and ''closed'' species. When the hydrogen bond opens, i.e. when the hydrogen bond breaks, the backbone amide proton involved in the hydrogen bond can exchange with the hydrogen of the solvent water. In EX2 limit [44], the stability of a given hydrogen bonded site as measured by the ratio of [CLOSED]/[OPEN], equals the protection factor. Thus, the protection factor is approximated as PF ≅ $1/K_{op}$. In our simulations, we have calculated protection factor during the equilibrium period by considering

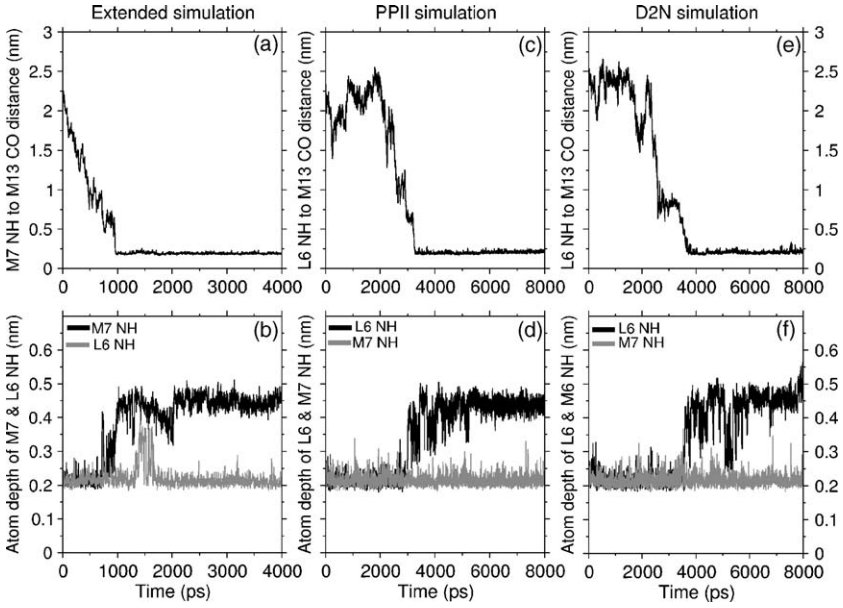

Fig. 8. Correlation between hydrogen bond formation involving amides (NH) of backbone and rise in atom depth values of these amides. (a) M7 NH to M13 CO distance as a function of time in Extended simulation. Hydrogen bond forms at about 1 ns when the distance falls below 0.26 nm. (b) Around the same time the atom depth value of M7 NH rises from ∼0.2 to 0.4 nm; L6 NH, which does not take part in backbone hydrogen bond, shows a steady value of atom depth at ∼0.2 nm during the same time period. Similarly as L6 NH takes part in hydrogen bonding with M13 CO, its atom depth rises to ∼0.4 nm whereas M7 NH, which does not take part in hydrogen bonding, shows a steady value for atom depth at 0.2 nm in PPII simulation (panels c, d) and in D2N simulation (panels e, f). For all the graphs a running average over 10 data points is plotted to reduce the level of fluctuations and enhance the visual clarity of the graphs.

Table 3
Atom depth values of all the amide protons with their standard deviations and protection factors of the amide protons taking part in hydrogen bonding interactions in various simulations are computed during the equilibrium period of 10–30 ns

Amide proton	Computed protection factor				Atom depth				Experimental protection factor[a]	
	Extended	PPII	D2N	ER	Extended	PPII	D2N	ER	Jacobs and Fox [16]	Walkenhorst et al. [17]
D2[b]	–	–	–	–	0.21 ± 0.03	0.22 ± 0.04	0.22 ± 0.04	0.22 ± 0.04	–	–
T3	–	–	–	–	0.24 ± 0.06	0.23 ± 0.04	0.23 ± 0.04	0.23 ± 0.04	46	0.61
V4	–	35	36[c]	–	0.25 ± 0.06	**0.43 ± 0.06**	**0.37 ± 0.09**	**0.30 ± 0.08**[d]	–	5.7
K5	22	–	–	8[e]	**0.42 ± 0.07**	0.21 ± 0.03	0.27 ± 0.09	**0.33 ± 0.06**	16	7.6
L6	–	56	31	387	0.21 ± 0.03	**0.45 ± 0.04**	**0.45 ± 0.04**	**0.46 ± 0.06**	42	6.8
M7	69	–	–	17	**0.44 ± 0.04**	0.21 ± 0.03	0.21 ± 0.03	**0.41 ± 0.05**	16	6.3
Y8	–	4	4	–	0.21 ± 0.03	**0.41 ± 0.06**	**0.42 ± 0.05**	0.20 ± 0.02	20	5.1
K9	1	–	–	–	**0.34 ± 0.11**	0.21 ± 0.03	0.21 ± 0.03	0.22 ± 0.03	–	–
G10	–	–	–	–	0.22 ± 0.03	0.22 ± 0.03	0.21 ± 0.03	0.21 ± 0.03	–	–
Q11	2	1	1	1	0.27 ± 0.06	**0.30 ± 0.06**	**0.30 ± 0.06**	0.28 ± 0.06	32	0.9
P12	–	–	–	–	–	–	–	–	–	–
M13	10	32	29	22	**0.42 ± 0.07**	**0.46 ± 0.04**	**0.46 ± 0.04**	**0.45 ± 0.06**	8.6	5.2
T14	–	–	–	–	0.22 ± 0.04	0.22 ± 0.04	0.22 ± 0.04	0.21 ± 0.03	–	–
F15	63	85	27	–	**0.44 ± 0.06**	**0.45 ± 0.04**	**0.42 ± 0.06**	0.22 ± 0.03	63	8.4
R16	–	–	–	26	0.21 ± 0.03	0.22 ± 0.04	0.24 ± 0.07	**0.42 ± 0.06**	–	16.2

Atom depth values greater than or equal to 0.3 nm are shown in bold.
[a] The numerical values of protection factors are taken from Jacobs and Fox [16] and from Walkenhorst et al. [17] (numerical values corresponding to reference [17] are obtained from Dr. W.F. Walkenhorst).
[b] This residue would be N2 in D2N simulation.
[c] The protection factor is computed for the equilibrium period of 20–30 ns, since the hydrogen bond (V4:H-F15:O) appears only after 20 ns.
[d] In these cases though computed protection factors are very small or close to zero, relatively larger atom depth values (≈0.30 nm) are observed possibly due to shielding of these amide protons from neighboring residues.
[e] The protection factor of K5 amide proton in ER simulation is computed from K5:H-Y8:OH hydrogen bond.

the number of frames in which the hydrogen bond is present (closed) and the number of frames in which a given hydrogen bond is broken (open) and taking the ratio of these numbers. These are listed in Table 3 and are in the range for molten globules (see later).

4. Discussion

4.1. The hydrogen bonding pattern observed in the simulations and atom depths of amide protons correlate with H–D exchange protection pattern experimentally observed in refolding experiments on staphylococcal nuclease

The hydrogen bonding pattern observed in the simulations and experimentally observed H–D exchange protection pattern are presented in the Table 4 along with atom depth values. The residues, which are known to be protected from H–D exchange in NMR experiments, are shown in gray boxes. These residues may have been protected from exchange either due to involvement of their backbone amide protons in hydrogen bonding interactions or due to solvent shielding of their amide protons. The amide protons, which are taking part in hydrogen bonding interactions in various simulations, are also shown in gray boxes. These residues can give rise to protection from H–D exchange by virtue of their participation in hydrogen bonding interactions. Further the amide protons whose computed atom depths are greater than ∼0.3 nm are shown in a solid box. It can be seen that those amides that take part in hydrogen bonding interactions are largely associated with atom depth values greater than ∼0.3 nm. Thus, there is a correlation between hydrogen bonding interactions and atom depths. This in turn leads to correlation between atom depths and H–D exchange protection. As can be judged from Table 4, the collection of trajectories observed in simulations will correlate with experimental observations in their H–D exchange protection patterns. We note that the participation of K9 in hydrogen bonding is observed in one of the simulations, but not in experiment. Though the amide proton of K9 takes part in hydrogen bonding interaction, its frequency is less (Table 3). Thus, K9 may not be observed in H–D exchange experiment as a protected residue. The residue T3 is observed to be protected in experiments. However, in our simulations the participation of T3 NH in a hydrogen bond is not observed.

We note that both native-like as well as non-native hydrogen bonding patterns (Fig. 3b) together only can account for experimental H–D exchange protection pattern. Thus, formation of non-native hairpins could also be on the folding pathway in the refolding of nuclease.

4.2. The computed atom depth values and the computed protection factors correlate well with each other

In Extended simulation, the computed protection factors of the amide protons that take part in hydrogen bonding interactions correlate with corresponding atom depth values with a correlation coefficient of 0.79. Correlation

Table 4
Comparison of experimental H–D exchange protection pattern with backbone amide proton's participation in hydrogen bonding interactions and its atom depths in various simulations during the equilibrium period of 10–30 ns

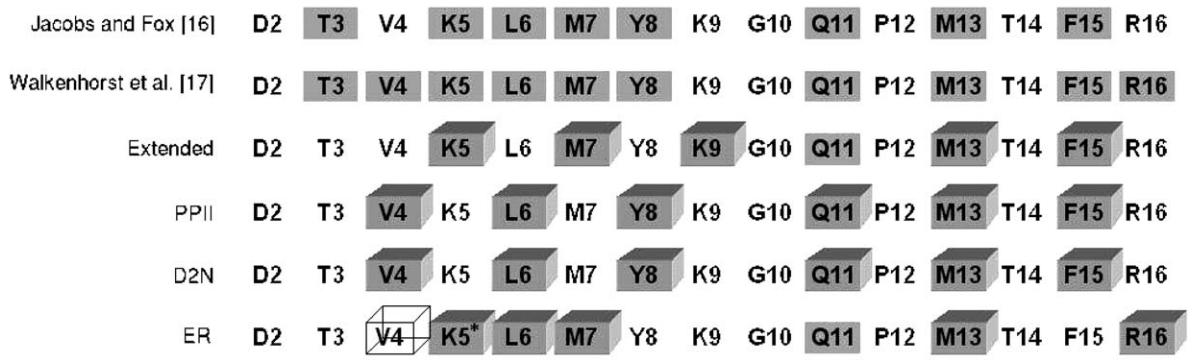

The experimental H–D exchange protection patterns from Jacobs and Fox [16] and Walkenhorst et al. [17] are displayed with gray boxes. The residues whose backbone amide protons take part in hydrogen bonding interactions in various simulations are also enclosed in gray boxes (see Fig. 3b for hydrogen bonding patterns observed in the simulations). In addition, the residues whose backbone amide protons, display an atom depth value greater than or equal to 0.3 nm are shown in a solid box (see also Table 3 for protection factors and atom depths of amide protons). *K5 amide proton in ER simulation is involved in K5:H-Y8:OH hydrogen bond.

coefficients of 0.81, 0.82, and 0.55 are observed, respectively, in PPII, D2N and ER simulations. These results imply that if the protection factor increases the corresponding atom depth also increases. Protection factors are related to the frequency of hydrogen bonding interactions, which in turn are related to the free energy of stabilization of the hydrogen bonds.

4.3. Hydrogen bond interactions seem to be stabilized by hydrophobic clusters

In the turn region, hydrogen bond is always weak in terms of the frequency of observation and this is reflected in atom depth values also (Table 3), since the turn is exposed to the solvent. In contrast, the hydrogen bonds in the middle of the hairpin are more frequent/stable and the corresponding amides have higher atom depth values (Table 3). We find that higher atom depth values arise from the association of hydrophobic residues, which shield the particular amide proton from the solvent. This suggests that the hydrogen bonding best takes place in a solvent shielded, low dielectric environment provided by the association/clustering of hydrophobic residues and only such hydrogen bonds are relatively more stable. Similar observations are made in a recent experimental study [45].

4.4. The hydrogen exchange protection factors computed from the simulations are characteristic for molten globule states and they agree qualitatively with experimental values

Alexandrescu et al. [44,46] studied a fragment of staphylococcal nuclease (1–103) corresponding to OB-fold with H–D exchange NMR. They find that amide protons from the β-sheet regions including the hairpin under study are among those protons with significant protection factors. The NMR structure of the fragment reveals that it has nuclease-like topology and structure though with reduced stability [46]. The observed protection factors range from 1 to 190 [44]. The hydrogen exchange protection factors obtained from NMR experiment of native proteins are usually in the range 10^3 to 10^6 or more [47] (Loh et al. [48] for example, give hydrogen exchange protection factors of ligated and unligated staphylococcal nuclease which are in the 10^3 to 10^6 range), whereas the protection factors obtained from refolding proteins in kinetic experiments usually are in the range of one to a few hundreds and may be considered small. For example, the protection factors obtained for nuclease during the refolding are in this range; in fact, they are less than even 100 [16,17]. We note that the molten globule state of α-lactalbumin is characterized by a maximum protection factor of 100 whereas its native state is characterized by a protection factors of the order 10^5 [49]. The protection factors computed from the simulations are small (Table 3) and thus are in the range for molten globule states.

It may be noted from Table 3 that there are significant differences between the protection factors reported by Jacobs and Fox [16] and Walkenhorst et al. [17]. While Jacobs and Fox [16] studied the mutant P117G, Walkenhorst et al. [17] studied the mutant H124L of nuclease. While both the studies conclude the early formation of β-hairpin region, the experimental protection factors differ in both the studies. Walkenhorst et al. [17] determined amide protection factors at a folding time of 16 ms, while Jacobs and Fox [16] used a folding time of 100 ms. Walkenhorst et al. [17] suggest that at these longer times more stable native-like species accumulate, leading to differences in the protection factors observed in both the experiments. However, there is overall agreement that β-sheet region is early to fold. Thus, for our purpose, the experimental protection factors give guidance as to whether a particular residue took part in early folding events or not. Accordingly, the computed protection factors from simulations need to be compared with the experimental protection factors keeping this

in mind. Thus, exact numerical agreement between computed protection factors with experimental protection factors is not necessary. The computed protection factors need only be similar to experimental protection factors in their orders of magnitude and such is found to be the case.

It may be noted that there is a variation in the values of computed protection factors from simulation to simulation (Table 3). The computed protection factors are the ratio of [CLOSED]/[OPEN] as discussed earlier. Thus, in a sense they represent the equilibrium constant for the formation and breaking of a hydrogen bond involving amide proton and carbonyl oxygen. Since equilibrium constant is related to free energy of hydrogen bond formation by $K = \exp(-\Delta G^{\circ}/RT)$, small variations in free energies of hydrogen bond formation will result in relatively larger changes in equilibrium constants or protection factors.

4.5. β-Hairpins form during the refolding experiments of staphylococcal nuclease

The hydrogen exchange experiments on nuclease have shown that the region corresponding to hairpin folded early and the experimental protection factors observed are small [16,17]. Since the computed protection factors for the folded hairpin exposed to the solvent too are small, it may be inferred that during the refolding of nuclease β-hairpins formed and displayed small protection factors. Note that H–D exchange experiments do not give information about the nature of the conformations sampled by the protected residues. Our simulations, therefore, complimented the experimental observations to suggest that formation of a β-hairpins did indeed take place during the refolding of nuclease. We further note that both native-like and non-native hairpins together alone can account for experimental observations.

4.6. Residues belonging to stable hydrophobic core of the nuclease are involved in the formation of the hairpin

Loh et al. [48] studied H–D exchange of amide protons in staphylococcal nuclease H124L both in ligated and unligated states. They find that most of the slowly exchanging hydrogens map to the central β-barrel and three most highly protected hydrogens map to strand 2 of the central 5-stranded β-barrel (K24, L25, M26 or K5, L6, M7 in our notation for the hairpin sequence). It can be seen from Table 4 that the residues K5, L6 and M7 take part in the formation of the hairpin both from experimental and simulation standpoints. Therefore, it seems that the residues belonging to a stable hydrophobic core, play a role in forming the hairpin and thus in initiating the folding of nuclease.

4.7. The major driving force for folding is hydrophobic interactions

The peptide folded into a hairpin conformation by various mechanisms in our simulations. We note that in Extended simulation, the hydrophobic contact between M7 and P12 takes place causing the loop formation. Following this event, other hydrophobic residues associate forming a compact hydrophobic cluster. Subsequently a hydrogen bond forms in the middle between M7 NH and M13 CO. Thus, the initial hydrophobic contact is an important event in nucleating the β-hairpin formation. In PPII and D2N simulations also, initial hydrophobic contact between Y8 and P12 played a role in initiating the hydrophobic association between opposite strands. However, in ER simulation, folding takes place following a second event of hydrophobic association after the formation and break up of a non-productive hydrophobic association. Thus, in all the simulations the major driving force for folding is hydrophobic interaction. We note that the nucleation of hairpin folding based on initial hydrophobic contact is to be followed by growth events of further hydrophobic associations. For example in ER simulation though the initial hydrophobic contact between Y8 and P12 takes place as early as 445 ps, the peptide does not fold as further hydrophobic association does not take place and the initial contact breaks up. Subsequently an unproductive hydrophobic association takes place without any hydrogen bonds. In a later event, the peptide unfolds again and a second event of hydrophobic association takes place, this time with the development of hydrogen bonds. Therefore, it appears that further consolidation of hydrophobic interaction requires supporting hydrogen bonding interactions. A similar observation is made by Prevost and Ortmans [12].

Thus, in the folding of the hairpin, the first step involves formation of a hydrophobic contact pair. The second step involves the growth of the hydrophobic cluster initially defined by the hydrophobic contact pair. The third step involves consolidation of hydrophobic interactions with supporting hydrogen bonding interactions. These are the common features in all the simulations. The only difference, which has been observed in ER simulation, is that an unproductive hydrophobic association takes place, which then breaks out as no supporting hydrogen bonds formed. It is difficult to correlate this observation to smaller box size, which of course has been chosen to be compatible with the dimensions of initial conformation and cut-off lengths. As mentioned earlier, supporting hydrogen bonds are required to consolidate hydrophobic interactions, a point noted by Prevost and Ortmann [12]. Once successful hydrophobic association takes place, further mechanism of folding is similar to other simulations.

4.8. Effect of box size and type on the results of simulations

In the ER simulation, the number of water molecules in the box is small in comparison to other simulations. In order to rule out the effect of smaller box size/less number of water molecules on the simulation results, we have carried out another simulation in an octahedron box containing 10,290 water molecules with initial extended conformation of the peptide (data not shown). The peptide folds into a hairpin in about 6 ns with non-native hydrogen bonding pattern. The overall mechanism of the folding is similar to other simulations in cubic boxes containing about 12,000–13,000 water

molecules. Thus, whether the box is cubic or octahedron the overall results of the simulations are similar. The unproductive hydrophobic association observed in ER simulation is not observed in any of the other simulations. While it may appear that the smaller box size may be a causative factor for the difference observed in ER simulation, there is nothing intrinsically unphysical about the mechanism of folding observed. Since the mechanism is not unphysical it may, in principle, be observable in a large number of simulations starting from various initial conditions.

4.9. Comparison to other simulations

Bonvin and Gunsteren [2] in some of their simulations on tendamistat, observed zip-up mechanism of β-hairpin folding, proposed by Munoz et al. [6,7]: a turn formed first, followed by formation of other hydrogen bonds in a zip-up manner from top-to-bottom, closing the hairpin. Subsequently stabilization of the hairpin is achieved by side chain hydrophobic interactions. In the case of PPII simulation, the mechanism of hairpin formation is found to be similar to the above mechanism, in that hydrogen bonds begin at the turn region and then propagate to the bottom of the hairpin.

In the Extended simulation, the formation of hydrophobic contact between M7 and P12 and subsequent association with other hydrophobic residues of opposite strands to form a hydrophobic cluster is an important initial event in the formation of the hairpin. Following this, the middle hydrogen bond M7:H-M13:O forms and the flanking hydrogen bonds form subsequently. Dinner et al. [4] also observed the formation of a hydrophobic cluster involving the middle residues on both the strands followed by propagation of hydrogen bonds outwards in both directions, which finally leads to the formation of the hairpin.

Ferrara and Caflisch [50] in their folding simulation of a three stranded antiparallel β-sheet peptide find that formation of contact between side chains close to the turn of the hairpin defined by strand 2 and 3 is an important folding event followed by consolidation events. In our simulation, too formation of contacts in the turn region is an important event in the folding of hairpin. Colombo et al. [51] in their study of β-hairpin formation find that the turn sequence and formation of hydrophobic nucleus favor the generation of β-hairpin. We also find that formation of loop/turn and hydrophobic association is an important element of folding mechanism. Ma and Nussinov [52] in their study of β-hairpin fragment of protein G by molecular dynamics find that hydrophobic interactions keep the peptide folded even in the presence of repulsive interactions between the strands. We too find that hydrophobic association between the strands contributes significantly to the stability of the folded state as discussed earlier.

4.10. Maintenance of turn hydrogen bond is not essential for sustaining hairpin conformation

In most of our simulations, we observed that the frequency of occurrence of hydrogen bonds is relatively less in the turn region of the hairpin as can be seen from Table 3. This suggests that the turn hydrogen bond is not essential for the maintenance of hairpin. The middle three hydrogen bonds are observed more frequently (Table 3). Once the middle hydrogen bonds form, both the strands are aligned and are associated with each other and the turn prefers to be an open turn without hydrogen bonds. Roccatano et al. [53] too find that the hydrogen bonds in the middle region of the hairpin are more stable than those in the turn and tail regions of the hairpin.

5. Conclusions

In the simulations, hairpins with both native-like and non-native hydrogen bonding are observed and can account for the experimental observations. Atom depth values are found to be reliable probes of the folded state of the amide protons that are solvent shielded/hydrogen bonded. They provide a direct way of inferring experimental H–D exchange protection patterns from simulations. Atom depths values and protection factors correlate well with the experimental protection factors. The formation of β-hairpin is found to be on the folding pathway in the refolding of staphylococcal nuclease. Hydrophobic interactions play an important role in the formation of hairpin. The hydrogen bonding best takes place in a solvent shielded, low dielectric environment provided by the association/clustering of hydrophobic residues.

Acknowledgements

We thank BRNS for funding the research through a research grant, sanction number 2001/37/18/BRNS/ 796, sanctioned to YUS and SP thanks BRNS for JRF fellowship. We thank Dr. M. Ramanadham for many helpful discussions and support. We thank Prof. S. Durani for critical reading of the manuscript.

References

[1] F. Blanco, M. Jiménez, J. Herranz, M. Rico, J. Santoro, J. Nieto, NMR Evidence of a short linear peptide that folds into a β-hairpin in aqueous solution, J. Am. Chem. Soc. 115 (1993) 5887–5888.
[2] A.M. Bonvin, W.F. van Gunsteren, beta-hairpin stability and folding: molecular dynamics studies of the first beta-hairpin of tendamistat, J. Mol. Biol. 296 (2000) 255–268.
[3] Z. Bryant, V.S. Pande, D.S. Rokhsar, Mechanical unfolding of a beta-hairpin using molecular dynamics, Biophys. J. 78 (2000) 584–589.
[4] A.R. Dinner, T. Lazaridis, M. Karplus, Understanding beta-hairpin formation, Proc. Natl. Acad. Sci. U.S.A. 96 (1999) 9068–9073.
[5] O.V. Galzitskaya, J. Higo, M. Kuroda, H. Nakamura, β-hairpin folds by molecular dynamics simulations, Chem. Phys. Lett. 326 (2000) 421–429.
[6] V. Munoz, P.A. Thompson, J. Hofrichter, W.A. Eaton, Folding dynamics and mechanism of beta-hairpin formation, Nature 390 (1997) 196–199.
[7] V. Munoz, E.R. Henry, J. Hofrichter, W.A. Eaton, A statistical mechanical model for beta-hairpin kinetics, Proc. Natl. Acad. Sci. U.S.A. 95 (1998) 5872–5879.
[8] V.S. Pande, D.S. Rokhsar, Molecular dynamics simulations of unfolding and refolding of a beta-hairpin fragment of protein G, Proc. Natl. Acad. Sci. U.S.A. 96 (1999) 9062–9067.
[9] H. Wang, J. Varady, L. Ng, S.S. Sung, Molecular dynamics simulations of beta-hairpin folding, Proteins 37 (1999) 325–333.

[10] X. Wu, S. Wang, B.R. Brooks, Direct observation of the folding and unfolding of a β-hairpin in explicit water through computer simulation, J. Am. Chem. Soc. 124 (2002) 5282–5283.
[11] X. Wu, B.R. Brooks, Beta-hairpin folding mechanism of a nine-residue peptide revealed from molecular dynamics simulations in explicit water, Biophys. J. 86 (2004) 1946–1958.
[12] M. Prevost, I. Ortmans, Refolding simulations of an isolated fragment of barnase into a native-like beta hairpin: evidence for compactness and hydrogen bonding as concurrent stabilizing factors, Proteins 29 (1997) 212–227.
[13] M.S. Searle, D.H. Williams, L.C. Packman, A short linear peptide derived from the N-terminal sequence of ubiquitin folds into a water-stable non-native beta-hairpin, Nat. Struct. Biol. 2 (1995) 999–1006.
[14] B. Zagrovic, E.J. Sorin, V. Pande, Beta-hairpin folding simulations in atomistic detail using an implicit solvent model, J. Mol. Biol. 313 (2001) 151–169.
[15] P.J. Loll, E.E. Lattman, The crystal structure of the ternary complex of staphylococcal nuclease, Ca2+, and the inhibitor pdTp, refined at 1.65 A, Proteins 5 (1989) 183–201.
[16] M.D. Jacobs, R.O. Fox, Staphylococcal nuclease folding intermediate characterized by hydrogen exchange and NMR spectroscopy, Proc. Natl. Acad. Sci. U.S.A. 91 (1994) 449–453.
[17] W.F. Walkenhorst, J.A. Edwards, J.L. Markley, H. Roder, Early formation of a beta hairpin during folding of staphylococcal nuclease H124L as detected by pulsed hydrogen exchange, Protein Sci. 11 (2002) 82–91.
[18] R.P. Chen, J.J. Huang, H.L. Chen, H. Jan, M. Velusamy, C.T. Lee, W. Fann, R.W. Larsen, S.I. Chan, Measuring the refolding of beta-sheets with different turn sequences on a nanosecond time scale, Proc. Natl. Acad. Sci. U.S.A. 101 (2004) 7305–7310.
[19] D. Du, Y. Zhu, C.Y. Huang, F. Gai, Understanding the key factors that control the rate of beta-hairpin folding, Proc. Natl. Acad. Sci. U.S.A. 101 (2004) 15915–15920.
[20] Y. Mu, D. Kosov, G. Stock, Conformational dynamics of trialanine in water. 2. Comparison of AMBER, CHARMM, GROMOS, and OPLS force fields to NMR and infrared experiments, J. Phys. Chem. B 107 (2003) 5064–5073.
[21] S. Woutersen, P. Hamm, Isotope-edited two-dimensional vibrational spectroscopy of a short alpha-helix in water, J. Chem. Phys. 114 (2001) 2727–2737.
[22] F. Eker, X. Cao, L. Nafie, R. Schweitzer-Stenner, Tripeptides adopt stable structures in water. A combined polarized visible Raman, FTIR, and VCD spectroscopy study, J. Am. Chem. Soc. 124 (2002) 14330–14341.
[23] Z. Shi, C.A. Olson, G.D. Rose, R.L. Baldwin, N.R. Kallenbach, Polyproline II structure in a sequence of seven alanine residues, Proc. Natl. Acad. Sci. U.S.A. 99 (2002) 9190–9195.
[24] A. Kentsis, M. Mezei, T. Gindin, R. Osman, Unfolded state of polyalanine is a segmented polyproline II helix, Proteins 55 (2004) 493–501.
[25] M. Mezei, P.J. Fleming, R. Srinivasan, G.D. Rose, Polyproline II helix is the preferred conformation for unfolded polyalanine in water, Proteins 55 (2004) 502–507.
[26] J. Chen, Z. Lu, J. Sakon, W.E. Stites, Increasing the thermostability of staphylococcal nuclease: implications for the origin of protein thermostability, J. Mol. Biol. 303 (2000) 125–130.
[27] N. Guex, M.C. Peitsch, SWISS-MODEL and the Swiss-PdbViewer: an environment for comparative protein modeling, Electrophoresis 18 (1997) 2714–2723.
[28] H. Berendsen, J.P.M. Postma, W.F. van Gunsteren, J. Hermans, Interaction models for water in relation to protein hydration, in: B. Pullman (Ed.), Inter Molecular Forces, Reidel Publishing Company, Dordrecht, The Netherlands, 1981, pp. 331–342.
[29] U. Essmann, L. Perera, M. Berkowitz, T. Darden, H. Lee, L. Pedersen, A smooth particle mesh Ewald method, J. Chem. Phys. 103 (1995) 8577–8593.
[30] T. Darden, D. York, L. Pedersen, Particle mesh Ewald: An N-log (N) method for Ewald sums in large systems, J. Chem. Phys. 98 (1993) 10089–10092.
[31] C. Sagui, T.A. Darden, Molecular dynamics simulations of biomolecules: long-range electrostatic effects, Annu. Rev. Biophys. Biomol. Struct. 28 (1999) 155–179.
[32] R.W. Hockney, J.W. Eastwood, Computer Simulation using Particles., McGraw-Hill, New York, 1981.
[33] B. Hess, H. Bekker, H.J.C. Berendsen, J.G.E.M. Fraaije, LINCS: a linear constraint solver for molecular simulations, J. Comput. Chem. 18 (1997) 1463–1472.
[34] H. Berendsen, J. Postma, A. DiNola, J. Haak, Molecular dynamics with coupling to an external bath, J. Chem. Phys. 81 (1984) 3684–3690.
[35] E. Lindahl, B. Hess, D. van der Spoel, Gromacs 3.0: a package for molecular simulation and trajectory analysis, J. Mol. Mod. 7 (2001) 306–317.
[36] W.F. van Gunsteren, S.R. Billeter, A.A. Eising, P.H. Hünenberger, P. Krüger, A.E. Mark, W.R.P. Scott, I.G. Tironi, Biomolecular Simulation: The GROMOS96 Manual and User Guide, Zürich, Switzerland, Hochschulverlag AG an der ETH Zürich, 1996.
[37] W.R.P. Scott, P. Huenenberger, I. Tironi, A. Mark, S. Billeter, J. Fennen, A. Torda, T. Huber, P. Krueger, W. van Gunsteren, The GROMOS biomolecular simulation program package, J. Phys. Chem. A 103 (1999) 3596–3607.
[38] X. Daura, K. Gademann, B. Jaun, D. Seebach, W.F. Van Gunsteren, A.E. Mark, Peptide folding: when simulation meets experiment, Angew. Chem. Int. Ed. 38 (1999) 236–240.
[39] W. Humphrey, A. Dalke, K. Schulten, VMD: visual molecular dynamics, J. Mol. Graph. 14 (1996) 33–38, 27–8.
[40] X. Daura, W.F. van Gunsteren, A.E. Mark, Folding-unfolding thermodynamics of a beta-heptapeptide from equilibrium simulations, Proteins 34 (1999) 269–280.
[41] A. Pintar, O. Carugo, S. Pongor, Atom depth as a descriptor of the protein interior, Biophys. J. 84 (2003) 2553–2561.
[42] A. Pintar, O. Carugo, S. Pongor, Atom depth in protein structure and function, Trends Biochem. Sci. 28 (2003) 593–597.
[43] T.G. Pedersen, B.W. Sigurskjold, K.V. Andersen, M. Kjaer, F.M. Poulsen, C.M. Dobson, C. Redfield, A nuclear magnetic resonance study of the hydrogen-exchange behaviour of lysozyme in crystals and solution, J. Mol. Biol. 218 (1991) 413–426.
[44] A.T. Alexandrescu, S.A. Dames, R. Wiltscheck, A fragment of staphylococcal nuclease with an OB-fold structure shows hydrogen-exchange protection factors in the range reported for ''molten globules'', Protein Sci. 5 (1996) 1942–1946.
[45] S. Deechongkit, H. Nguyen, E.T. Powers, P.E. Dawson, M. Gruebele, J.W. Kelly, Context-dependent contributions of backbone hydrogen bonding to beta-sheet folding energetics, Nature 430 (2004) 101–105.
[46] A.T. Alexandrescu, A.G. Gittis, C. Abeygunawardana, D. Shortle, NMR structure of a stable ''OB-fold'' sub-domain isolated from staphylococcal nuclease, J. Mol. Biol. 250 (1995) 134–143.
[47] T.M. Raschke, S. Marqusee, Hydrogen exchange studies of protein structure, Curr. Opin. Biotechnol. 9 (1998) 80–86.
[48] S.N. Loh, K.E. Prehoda, J. Wang, J.L. Markley, Hydrogen exchange in unligated and ligated staphylococcal nuclease, Biochemistry 32 (1993) 11022–11028.
[49] B.A. Schulman, C. Redfield, Z.Y. Peng, C.M. Dobson, P.S. Kim, Different subdomains are most protected from hydrogen exchange in the molten globule and native states of human alpha-lactalbumin, J. Mol. Biol. 253 (1995) 651–657.
[50] P. Ferrara, A. Caflisch, Folding simulations of a three-stranded antiparallel beta-sheet peptide, Proc. Natl. Acad. Sci. U.S.A. 97 (2000) 10780–10785.
[51] G. Colombo, G.M. De Mori, D. Roccatano, Interplay between hydrophobic cluster and loop propensity in beta-hairpin formation: a mechanistic study, Protein Sci. 12 (2003) 538–550.
[52] B. Ma, R. Nussinov, Molecular dynamics simulations of a beta-hairpin fragment of protein G: balance between side-chain and backbone forces, J. Mol. Biol. 296 (2000) 1091–1104.
[53] D. Roccatano, A. Amadei, A. Di Nola, H.J. Berendsen, A molecular dynamics study of the 41–56 beta-hairpin from B1 domain of protein G, Protein Sci. 8 (1999) 2130–2143.